2021 43rd Annual International Conference of the
IEEE Engineering in Medicine & Biology Society (EMBC)
Oct 31 - Nov 4, 2021. Virtual Conference

Non-Invasive Microwave Hyperthermia and Simultaneous Temperature Monitoring with a Single Theranostic Applicator*

Gertjan Maenhout[1], Tomislav Markovic[1,2], and Bart Nauwelaers[1]

***Abstract*— Cancer therapies are constantly evolving. Currently, heating tumor tissue is becoming more accessible as a stand-alone method or in combination with other therapies. Due to its multiple advantages over other heating mechanisms, microwave hyperthermia has recently gained a lot of traction. In this work, we present a complementary split-ring resonator that is simultaneously excited in two independent frequency bands. With a high-power signal, the applicator is excited and heats the tissue-under-test up to 50°C with an average heating rate of 0.72°C per second. Furthermore, we present a dielectric temperature control system using the same applicator for microwave hyperthermia applications, which currently still requires an additional thermometry system. By exciting the applicator with a low-power signal, we can constantly monitor its resonant frequency. This resonant frequency depends on the tissue properties, which in turn are temperature-dependent. In the temperature range from 20−50°C, a positive correlation between the temperature and resonant frequency was established.**

***Clinical relevance* – Exploiting the dual-band behavior of the complementary split-ring resonator to heat the tissue-under-test while dielectrically monitoring its temperature, creates new possibilities towards a theranostic, non-invasive microwave hyperthermia applicator.**

I. Introduction

Cancer is currently the second-highest cause of death worldwide. Therefore, multiple methods have been developed regarding cancer treatment. Conventional methods, e.g. surgery or chemotherapy, are constantly improving, novel methods, e.g. immunotherapy or gene therapy, are gradually introduced, and a promising solution lies in the combination of several of these methods. One of these novel methods focuses on heating the tumor tissue or tissue-under-test (TUT) for a long period of time (30−60 minutes). With hyperthermia therapy, the TUT is exposed to temperatures of 41 to 45°C which render the tumor more sensitive to other treatments. At temperatures above $45-47$°C, thermal ablation directly abolishes the TUT [1], [2].

Hyperthermia therapy can be administered with high-intensity ultrasound, laser heating, or with electromagnetic (EM) microwave heating. EM heating is generally divided in radiofrequency ablation (RFA) with an operating frequency around 350−500 kHz and microwave ablation (MWA) typically operating in the 900−2500 MHz range. Recently the use of MWA has attracted more attention due to several advantages: (1) MWA typically performs better at heating a larger TUT, (2) it has the possibility to heat tissue further away from the applicator, and (3) the heating procedure is typically faster than RFA since it relies on direct heating instead of thermal conductance [3], [4].

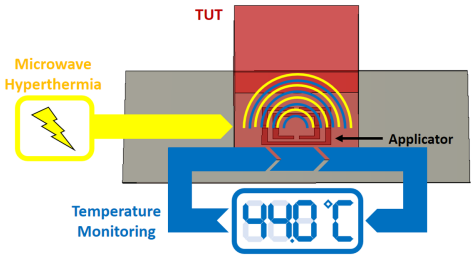

Fig. 1: A graphical sketch of this work where a single applicator is excited with two EM signals: one for heating the TUT, and the other for monitoring its temperature.

However, the effect of the hyperthermia treatment is predominantly determined by the TUT temperature and the time of the procedure. Studies suggest that a change of 1°C can be equivalent to a change in heating time by a factor of six [5]. Therefore, temperature control of the treated zone is imperative. This can be accomplished using invasive temperature probes located close to the TUT, with magnetic resonance (MR) thermometry, or with thermal utrasound imaging [6], [7]. In this work, we present a dual-band, EM microwave hyperthermia applicator that simultaneously acts as a temperature sensor and monitors the temperature of the TUT as graphically represented in Fig. 1. The TUT in this work is a homogeneous sample but with proper calibration [8], [9] the technique can be adjusted to multi-layered tissues. Section II describes the design process of the sensor as well as its heating and sensing operation. The proposed measurement setup and the used materials are presented in section III. Lastly, the obtained experimental results are shown in section IV.

II. Sensor Design and Methods

A. Complementary Split-Ring Resonator

Metamaterial-based transmission lines have been widely used to modify the characteristic impedance and dispersion of transmission lines [10]. These transmission lines are typically loaded with reactive components or with small resonators. Several of these topologies have recently been used successfully as a sensing structure [11] or as a dual detector-heater applicator [12].

* This work is supported in part by the Research Foundation Flanders (FWO) SB PhD fellowship under grant number 1S23918N (G. Maenhout).
[1] G. Maenhout, T. Markovic, and B. Nauwelaers are with the Department of Electrical Engineering (ESAT), KU Leuven, Kasteelpark Arenberg 10, Box 2444, 3001, Leuven, Belgium.
[2] T. Markovic is also with imec, Kapeldreef 75, 3001 Heverlee, Belgium.

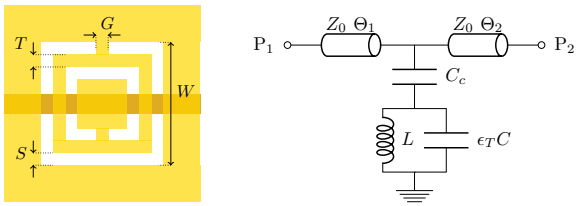

(a) (b)

Fig. 2: **(a)** Detailed schematic of the CSRR (transparent gold) with width W, spacing S, trace width T, and gap G, and the underlying microstrip transmission line (brown). **(b)** The equivalent electrical circuit of the CSRR.

One of these topologies is the complementary split-ring resonator (CSRR). It is a two-layer, planar structure that consists of a defected ground plane that is excited by a transmission line. A schematic drawing of a CSRR with its design parameters is shown in Fig. 2a. Its equivalent electrical scheme is shown in Fig. 2b. It incorporates a parallel resonant circuit, which is capacitively coupled to a transmission line [13]. When a TUT is placed on the defected ground plane, the capacitor C is altered by the tissue properties and it can be represented as a lossy capacitor:

$$\epsilon_T C = (\epsilon'_T + j\epsilon''_T)C. \tag{1}$$

Due to its electrical field distribution, perpendicular to the sensor plane, EM waves can penetrate deep into the TUT. In our previous work [14], we concluded that the CSRR is a promising sensing topology: for a design with $W = 5$ mm, $G = 0.4$ mm, $S = 0.4$ mm, and $T = 0.4$ mm, a sensitivity of -20.7 MHz per a.u. of ϵ'_T was established over a broad permittivity range, the sensor can penetrate up to 6 mm into the TUT, and it can reach a spatial resolution of 2 mm.

B. Microwave Heating for Hyperthermia

The heating of the TUT with microwaves relies on the principle of dielectric heating. By applying an alternating electrical field, electrical dipoles start to rotate to align themselves along the imposed electrical field. This rotation causes friction between the dipoles, which generates heat. The amount of energy that is converted into heat heavily depends on the amount of friction in the TUT, which is characterized by the imaginary part of its dielectric permittivity ϵ''_T. With regards to biological tissue, ϵ''_T is largely determined by the water content of the tissue. Therefore, dielectric heating yields better results in tissues with a higher water content such as muscle tissue opposed to adipose tissue.

When port P_2 of the equivalent circuit is left open, a standing wave pattern is created in the structure. The standing wave can be further analyzed by observing the input impedance Z_{IN} at port P_1:

$$Z_{\text{IN}} = \frac{Z_{\text{CSRR}} \cdot Z_{\text{TLIN2}}}{Z_{\text{CSRR}} + Z_{\text{TLIN2}}}, \tag{2}$$

with

$$Z_{\text{CSRR}} = \frac{1}{j\omega C_c} + \frac{j\omega L}{1 - \omega^2 L \epsilon_T C} \tag{3}$$

$$Z_{\text{TLIN2}} = \frac{Z_0}{j\tan(\Theta_2)}. \tag{4}$$

When Z_{IN} is equal to the characteristic impedance Z_0, the structure is matched at this frequency ($f_{\text{m.}}$) and the maximum amount of power is accepted. This power is dissipated in the lossy components of the structures, i.e. the lossy capacitor $\epsilon_T C$, which results in the heating of the TUT.

The structure was simulated in a high frequency-thermal co-simulation in CST Microwave Studio. The structure was loaded with muscle tissue and its dielectric data where provided by [15]. A matched impedance was observed at 4.17 GHz. Next, the obtained power losses were used in a thermal simulation. The heat transfer was modelled with Pennes bioheat equation that incorporates the effects of metablism and blood perfusion [16]. The relevant thermal properties of muscle tissue were found in [17], [18]. Lastly, the data was exported to Matlab were it was further analyzed.

With a 1.5 W input signal at $f_{\text{m.}} = 4.17$ GHz, a maximum temperature of 48.5°C was obtained within 250 sec. Fig. 3 shows the simulated isotherms in the muscle tissue and a 4.5 $\times$ 3.5 $\times$ 6 mm^3 hyperthermia zone was established in which temperatures exceeded 45°C.

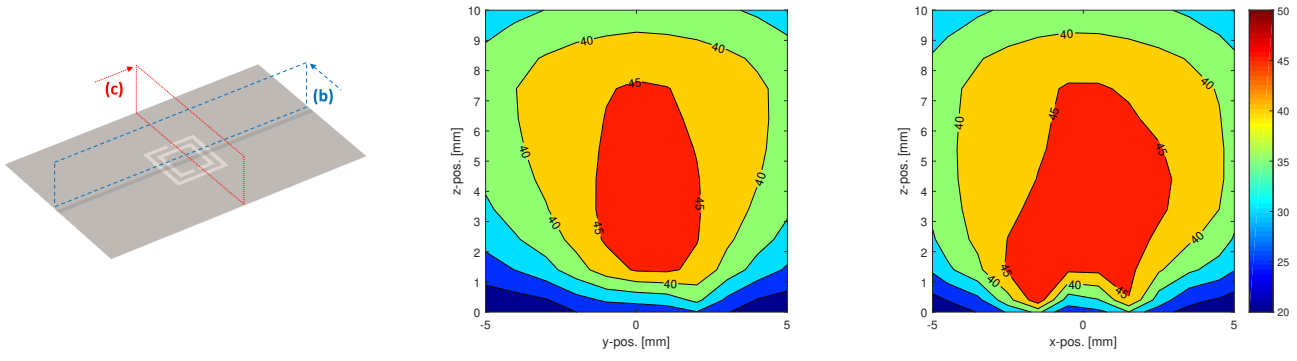

(a) (b) (c)

Fig. 3: The isotherms throughout the TUT along the cutting planes as defined in **(a)**. The isotherms at the cutting plane parallel to the transmission line in **(b)**, and the isotherms at the cutting plane perpendicular to the transmission line in **(c)**.

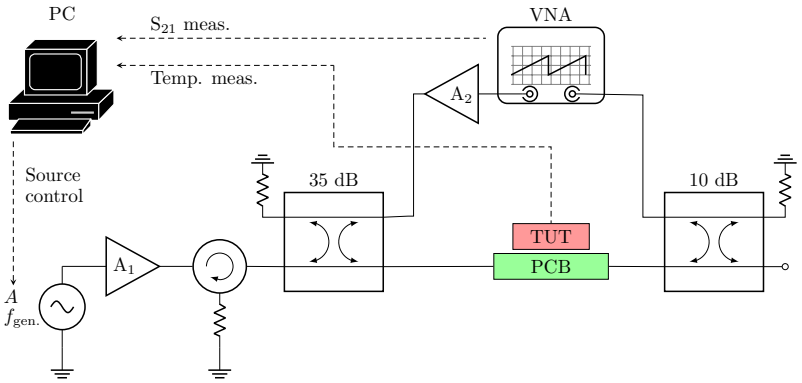

Fig. 4: A schematic overview of the proposed setup to simultaneously heat the TUT and monitor its temperature through the analysis of the S_{21} of the CSRR. (All dashed lines carry data and all drawn resistors are 50 Ω terminations.)

C. Dielectric Temperature Monitoring

When analyzing the sensing topology in detail, an additional TUT-dependent series resonance can be observed:

$$f_{\text{res.}} = \frac{1}{2\pi\sqrt{(C_c + \epsilon_T C) \times L}}. \tag{5}$$

At $f_{\text{res.}}$, a short is introduced to the transmission line. This can be detected in the transmission coefficient S_{21} as a transmission zero. Since several studies [19], [20] demonstrated that a change in temperature of the TUT has a direct impact on the ϵ'_T of the TUT, it is possible to dielectrically monitor the TUT temperature by tracking the $f_{\text{res.}}$. In other words, a temperature increase will result in a decrease of ϵ'_T, resulting in an increase of $f_{\text{res.}}$.

Additionally, by simply varying Θ_2, the system can be designed such that a difference exists between $f_{\text{m.}}$ and $f_{\text{res.}}$. This enables the implementation of a dual-mode setup. The TUT can be heated by applying a high-power signal at frequency $f_{\text{m.}}$. Simultaneously, a vector network analyzer (VNA) can inject a second low-power signal in the system to track changes in $f_{\text{res.}}$, allowing a dielectric monitoring of the TUT temperature. In conclusion, one single applicator can simultaneously heat the TUT and monitor its temperature.

III. Measurement Setup and Materials

A 0.25 mm Rogers 4350B substrate was selected and the CSRR was manufactured on a printed circuit board (PCB) with standard manufacturing techniques. Two subminiature version A (SMA) connectors were soldered onto the PCB to enable the connection to the measurement equipment. The TUT was placed on top of the PCB and was shielded from its surroundings using a polymethylmethacrylate (PMMA) enclosure to prevent dehydration [21].

The schematic in Fig. 4 demonstrates the implementation of the proposed setup. The PC can automatically control the amplitude A and frequency $f_{\text{gen.}}$ of the signal generator (MXG N5182B, Keysight Technologies). This signal is fed to amplifier A_1 (2-8 GHz/4 W, BSW Test System & Consulting) to generate a high-power signal to heat the TUT. Note that the 10 dB directional coupler can be represented as an extension of Θ_2. As a consequence, the matched frequency shifted to 5.15 GHz. A T-type thermocouple was inserted in the TUT and was connected to the PC through a NI-TC01 temperature reader. The temperature was further supplied to a PI-controller in Matlab that regulated the amplitude A of the source to obtain a stable TUT temperature.

Additionally, a second low-power path to the PCB was created through two directional couplers. A VNA (FieldFox N9917A, Keysight Technologies) was connected to this path in order to measure S_{21} of the CSRR. An extra amplifier A_2 (83050A, HP) was added to compensate for the losses of the directional couplers in this path and to keep the measurement signal above the noise floor. The transmission measurements were conducted in the 3.5−3.6 GHz range with a frequency step of 1 MHz. The output power was set at 3 dBm and an IFBW of 1 kHz was used. The S_{21} data was saved on the PC and synchronized with the temperature data.

These experiments were conducted on fresh bovine muscle samples that were purchased at a local grocery shop. The samples were allowed to reach room temperature and were sliced into a $9 \times 9 \times 8$ mm^3 shape right before they were placed in the PMMA enclosure in direct contact with the PCB. Despite their degradation over time, the use of these samples was favored over tissue phantoms since no phantoms are known that simultaneously have (1) a similar permittivity over a broad frequency range, (2) a similar change in permittivity due to temperature changes, and (3) similar thermal properties in order to mimic heating.

IV. Experimental Results

To demonstrate the heating capabilities of the setup, six, linearly spaced, different temperature setpoints were selected in the 25−50°C temperature range. At each setpoint, the heating experiment was repeated five times with five different samples for further statistical analysis. When the set temperature was reached, the sample was kept at this temperature for 5 minutes. Fig. 5 shows the obtained heating rates for the six different temperatures. The PI-controller sets the amplitude A of the exciting signal and the TUT rapidly reaches the desired temperature at an average heating rate of 0.72°C per sec. A slight overshoot of maximum 3.5°C can be observed

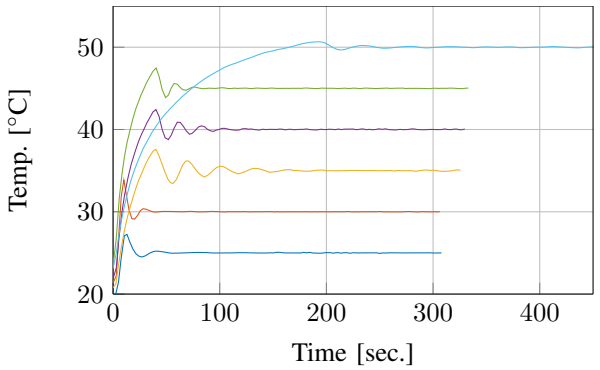

Fig. 5: The temperature of the TUT throughout six different experiments, each at a different set temperature.

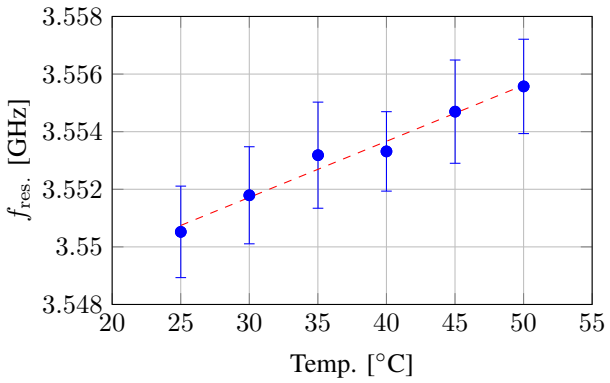

Fig. 6: The average $f_{\text{res.}}$ at the six different temperatures with their corresponding standard deviation and a linear fit $\left(f_{\text{res.}} = 3.545\ [\text{GHz}] + T \times 0.195\ \left[\frac{\text{MHz}}{^\circ\text{C}}\right]\right)$.

but the temperature rapidly stabilizes within 3 oscillations after which a standard deviation of 0.12°C is measured.

Throughout the heating procedure, the VNA recorded the S_{21} of the CSRR each second. A resonance was observed with a quality factor of 54.7±2.6 across all measurements [22]. The mean $f_{\text{res.}}$ from all measurements of the five samples at a single temperature was calculated along with its standard deviation. The relation between TUT temperature and the corresponding $f_{\text{res.}}$ is shown in Fig. 6. Here we can clearly observe a positive correlation between temperature and $f_{\text{res.}}$. Furthermore, due to the non-overlapping error bars, we can claim that the difference in $f_{\text{res.}}$ is statistically significantly different.

V. Conclusion and Future Work

This paper presented a theranostic applicator that exploited its structure at two separate and independent frequencies. At the matched frequency $f_{\text{m.}}$, a high-power signal excited the CSRR and heated the TUT. A 4.5 × 3.5 × 6 mm^3 hyperthermia zone, in which temperatures exceeded 45°C, was established in CST simulations and a rapid heating rate of 0.72°C per sec. was measured in experiments conducted on bovine muscle tissue. Secondly, the resonant frequency $f_{\text{res.}}$, dependent on the dielectric properties of the TUT ϵ_T, was simultaneously tracked with a low-power signal and was correlated with the TUT temperature. In future work, the sensitivity of the temperature readout can be improved by inserting an isolation layer between the TUT and the PCB at the cost of a decreased heating efficiency.

References

[1] J. Beik *et al.*, "Nanotechnology in hyperthermia cancer therapy: From fundamental principles to advanced applications," *J. Control. Release*, vol. 235, pp. 205–221, 2016.

[2] M. Puentes *et al.*, "Planar microwave sensor for thermal ablation of organic tissue," in *2013 European Microwave Conference*, pp. 479–482, Oct 2013.

[3] K. F. Chu and D. E. Dupuy, "Thermal ablation of tumours: biological mechanisms and advances in therapy," *Nat. Rev. Cancer*, vol. 14, no. 3, pp. 199–208, 2014.

[4] C. Kim, "Understanding the nuances of microwave ablation for more accurate post-treatment assessment," *Future Oncol.*, vol. 14, no. 17, pp. 1755–1764, 2018.

[5] S. Field and C. Morris, "The relationship between heating time and temperature: its relevance to clinical hyperthermia," *Radiother. Oncol.*, vol. 1, no. 2, pp. 179–186, 1983.

[6] G. Bruggmoser *et al.*, "Quality assurance for clinical studies in regional deep hyperthermia," *Strahlenther. Onkol.*, vol. 187, no. 10, pp. 605–610, 2011.

[7] Y. Hadadian *et al.*, "A novel theranostic platform: Integration of magnetomotive and thermal ultrasound imaging with magnetic hyperthermia," *IEEE Trans. Biomed. Eng.*, vol. 68, pp. 68–77, Jan 2021.

[8] L. P. Yan *et al.*, "A noninvasive method for determining dielectric properties of layered tissues on human back," *J. Electromagn. Waves Appl.*, vol. 21, no. 13, pp. 1829–1843, 2007.

[9] S. Huclova *et al.*, "Sensitivity and specificity analysis of fringing-field dielectric spectroscopy applied to a multi-layer system modelling the human skin," *Phys. Med. Biol.*, vol. 56, no. 24, pp. 7777–7793, 2011.

[10] R. Marques *et al.*, *Metamaterials with negative parameters: theory, design, and microwave applications*. Wiley-Interscience, 2013.

[11] C. Lee and C. Yang, "Complementary split-ring resonators for measuring dielectric constants and loss tangents," *IEEE Microw. Wirel. Compon. Lett.*, vol. 24, pp. 563–565, Aug 2014.

[12] C. Reimann *et al.*, "Planar microwave sensor for theranostic therapy of organic tissue based on oval split ring resonators," *Sensors*, vol. 16, no. 9, 2016.

[13] J. D. Baena *et al.*, "Equivalent-circuit models for split-ring resonators and complementary split-ring resonators coupled to planar transmission lines," *IEEE Trans. Microw. Theory Tech.*, vol. 53, pp. 1451–1461, Apr 2005.

[14] G. Maenhout *et al.*, "Complementary split-ring resonator with improved dielectric spatial resolution," *IEEE Sens. J.*, vol. 21, no. 4, pp. 4543–4552, 2020.

[15] S. Gabriel *et al.*, "The dielectric properties of biological tissues: III. parametric models for the dielectric spectrum of tissues," *Phys. Med. Biol.*, vol. 41, pp. 2271–2293, Nov 1996.

[16] H. H. Pennes, "Analysis of tissue and arterial blood temperatures in the resting human forearm," *J. Appl. Physiol.*, vol. 1, no. 2, pp. 93–122, 1948.

[17] P. Hasgall *et al.*, "Database of tissue properties." 10.13099/VIP21000-04-0, May 2018. Version 4.0.

[18] A. Hirata *et al.*, "Correlation between peak spatial-average sar and temperature increase due to antennas attached to human trunk," *IEEE. Trans. Biomed. Eng.*, vol. 53, no. 8, pp. 1658–1664, 2006.

[19] M. Lazebnik *et al.*, "Ultrawideband temperature-dependent dielectric properties of animal liver tissue in the microwave frequency range," *Phys. Med. Biol.*, vol. 51, pp. 1941–1955, Mar 2006.

[20] M. Ngadi *et al.*, "Dielectric properties of pork muscle," *Int. J. Food Prop.*, vol. 18, no. 1, pp. 12–20, 2015.

[21] G. Maenhout *et al.*, "Effect of dehydration on dielectric measurements of biological tissue as function of time," *IEEE J. Electromagn., RF, Microw. Med. Biol.*, vol. 4, no. 3, pp. 200–207, 2020.

[22] L. F. Chen *et al.*, *Microwave Electronics: Measurement and Materials Characterization*, p. 135. John Wiley & Sons, 2005.